

# Liquid transportation fuels from biomass-derived oxygenates: Gas-phase 2-hexanol upgrading on Cu-based mixed oxides



P.J. Luggren, C.R. Pesteguía, J.I. Di Cosimo\*

Catalysis Science and Engineering Research Group (GICIC), INCAPe, UNL-CONICET, Santiago del Estero 2654, 3000 Santa Fe, Argentina

## ARTICLE INFO

### Article history:

Received 1 October 2014

Received in revised form

29 December 2014

Accepted 5 January 2015

Available online 12 January 2015

### Keywords:

2-Hexanol  
Aldol condensation  
Dehydrogenation  
Hydrogenation  
Copper  
Mixed oxides

## ABSTRACT

The gas-phase upgrading of 2-hexanol, a model molecule of the primary conversion of sugars, toward higher molecular weight compounds of application as liquid transportation fuels was investigated on Cu–M<sub>I</sub>–M<sub>II</sub> mixed oxides (M<sub>I</sub>, M<sub>II</sub>: Mg<sup>2+</sup>, Al<sup>3+</sup>, Ce<sup>4+</sup>) at 573 K and 101.3 kPa. Catalysts were prepared by coprecipitation and characterized by several techniques such as BET surface area, XRD, TPD of CO<sub>2</sub> and NH<sub>3</sub>, TPR and N<sub>2</sub>O decomposition. The bifunctional metal–base catalytic process occurs through a series of sequential steps comprising dehydrogenation, C–C coupling, dehydration and hydrogenation reactions. Nano-sized Cu<sup>0</sup> particles promote dehydrogenation and hydrogenation steps whereas acid–base sites provided by M<sub>I</sub>(M<sub>II</sub>)–O pairs participate in the C–C coupling reaction. In general, main products were C9–C12 compounds that represented ~60% of the product pool. Branched C9–C24 compounds such as ketones, alcohols and alkanes were obtained with yields of up to 91% on a Cu–Mg–Al mixed oxide with 8 wt.% Cu (catalyst 8.0CuMgAl). This catalyst presented well dispersed Cu<sup>0</sup> particles and a high number of base sites with moderate basic properties as well as a low number of acid sites. The rate-limiting step of the bifunctional process leading to C9–C24 products on catalyst 8.0CuMgAl was the metal-promoted hydrogenation step, but the reaction can be controlled by the C–C bond formation step on less basic catalysts. By carrying out experiments under different reaction atmospheres (N<sub>2</sub> or H<sub>2</sub>) and at different contact times, a reaction pathway leading to formation of odd carbon atom number products (C9, C15 and C21) is postulated in contrast to the conventional aldol condensation pathway toward even carbon atom number products (C12, C18 and C24). The former prevails under conditions at which the catalyst surface is deprived of hydrogen atoms.

© 2015 Elsevier B.V. All rights reserved.

## 1. Introduction

In the last decades, several factors have prompted the development of new technologies for energy production: (i) the growth of emerging economies; (ii) the energy consumption increase, (iii) the diminution of conventional petroleum resources; (iv) the slow process of investment and development of non-conventional resources (shale gas and shale oil); (v) the increasing environmental concern about climate change.

The “integrated biorefineries” and the development of new technologies based on renewable resources are an attractive option to produce liquid transportation fuels and chemicals [1,2]. For example, lignocellulose, the most abundant carbohydrate in nature, is an inexpensive feedstock but processing of this material is difficult.

Different thermal, chemical and biological processes have been postulated for breaking down lignocellulose into chemical species that are easier to process. In particular, lignocellulose can be transformed in sugars by acid hydrolysis. Then, conversion of sugars in the biorefinery results in the production of liquid alkanes [3,4]. The main advantages of the biofuels derived from carbohydrates are that they can be synthesized from abundant resources that do not compete with food supply and that their combustion has a zero CO<sub>2</sub> balance. However, to obtain second generation liquid biofuels with proper physical and combustion properties is challenging. Sugars are C5–C6 compounds with high oxygen content (C:O = 1:1). This chemical composition is inadequate for liquid transportation fuel applications which consist of nonoxygenated hydrocarbons in the range of C5–C12 for gasoline, C9–C16 for jet fuel and C12–C20 for diesel [5]. Thus, conversion of sugars into liquid fuels in the biorefinery requires removal of almost all the oxygen atoms from the molecules by hydrolysis, dehydration or hydrogenation reactions [4,6]. In addition to deoxygenation, other processes must take place such as isomerization to form branched hydrocarbons

\* Corresponding author. Tel.: +54 342 4511546x1558; fax: +54 342 4511170.  
E-mail address: [dicosimo@fiq.unl.edu.ar](mailto:dicosimo@fiq.unl.edu.ar) (J.I. Di Cosimo).

for gasoline, and/or by C–C coupling reactions to increase the molecular weight for diesel and jet fuels [6].

In 2008, Kunkes et al. [6] postulated a strategy to convert carbohydrates in liquid fuels. The strategy starts by oxygen removal from sugars and polyols at 500 K on a Pt-Re/C catalyst to yield a well-defined mixture of hydrophobic species consisting of mono-functional oxygenates containing 4–6 carbon atoms. More than 80% of the oxygen contained in the carbohydrate is removed in this catalytic step. An advantage of this strategy is that the hydrophobic mixture comprises the so called “platform molecules”, such as ketones, carboxylic acids, secondary alcohols and heterocyclic compounds (furans). These compounds can be further transformed into C9–C18+ alkanes to be used as liquid transportation fuels. In particular, Kunkes et al. [6] also demonstrated that bifunctional Cu–Mg–Al mixed oxides previously developed in our group [7] were suitable catalysts for the subsequent upgrading of this C4–C6 organic liquid stream to C6–C12 compounds. They showed that at 573 K, 5 bar of pressure and cofeeding H<sub>2</sub>, 45% of the carbon in the product mixture is associated with C8–C12 condensation products containing one or none oxygen atoms.

Cu–Mg–Al mixed oxide catalysts have been also successfully used in other applications requiring a combination of metallic and acid–base sites. For example, we showed that conversion of alcohols, such as 2-propanol, proceeds at high rates on these catalysts by a sequence of steps that comprises dehydrogenation–aldol condensation–dehydration–hydrogenation reactions [7,8]. Furthermore, we found that gas-phase reduction of α,β-unsaturated ketones by hydrogen transfer reactions selectively forms saturated ketones on these catalysts [9]. We reported also that these materials promote the upgrading of polyols to valuable oxygenates by dehydrogenation and/or dehydration reactions, depending on the copper loading [10]. Recently, other researchers have shown that similar Cu–Mg–Al mixed oxides are suitable catalysts for C–C coupling of methanol and ethanol [11], aqueous-phase upgrading of bio-oil [12], total oxidation of methane [13] and synthesis of 1,2-propanediol from glycerol [14] among many other applications.

In this work we investigate the synthesis of liquid transportation fuels using 2-hexanol as a model “platform molecule” derived from sugars, according to the above-mentioned strategy [6]. The gas-phase conversion of 2-hexanol was carried out at atmospheric pressure and mild reaction temperatures (573 K). Formation of C9–C24 oxygenates and hydrocarbons from 2-hexanol involves tandem dehydrogenation–C–C coupling–dehydration–hydrogenation reactions. We report the catalytic results obtained with Cu-containing mixed oxides that combine a well dispersed metallic function provided by copper with moderate acid–base properties. The bifunctional nature of the catalytic process is discussed as well as the role played by each active site in the reaction sequence. The reaction pathways are elucidated by carrying out catalytic experiments under different conditions. The effect of cofeeding H<sub>2</sub> on the product distribution and on the shift of the reaction pathway is also reported. The rate-limiting steps operating in catalysts with different relative abundance of metal and acid–base sites are postulated.

## 2. Experimental

### 2.1. Catalyst synthesis and characterization

Catalyst precursors of binary M<sub>I</sub>M<sub>II</sub>, or Cu-containing ZCuM<sub>I</sub>(M<sub>II</sub>) mixed oxides, where M<sub>I</sub> and M<sub>II</sub> are metal cations such as Mg<sup>2+</sup>, Al<sup>3+</sup>, or Ce<sup>4+</sup> and Z stands for the copper content in wt.%, were prepared by coprecipitation under similar conditions, as detailed elsewhere [7]. Z was 6–10 wt.% in Cu-based catalysts. As an example, the ternary Cu–Mg–Al catalyst precursor with a Mg/Al = 1.5 molar ratio was prepared by co-precipitation at a

constant pH of 10. After filtering, washing and drying at 363 K, the precipitate was decomposed overnight in air at 773 K in order to obtain the corresponding mixed oxide, 8.0CuMgAl. Following similar calcination procedures Mg–Ce, Cu–Mg, Cu–Ce, Cu–Al and Cu–Mg–Ce catalysts were obtained, which were denoted as MgCe, 9.8CuMg, 7.4CuCe, 6.4CuAl and 6.9CuMgCe, respectively. High-surface area magnesium oxide was prepared by hydration with distilled water of low-surface area commercial MgO (Carlo Erba 99%; 27 m<sup>2</sup>/g) and further decomposition of the resulting Mg(OH)<sub>2</sub> in a N<sub>2</sub> flow for 18 h at 773 K [15]. Alumina and ceria were commercial samples of γ-Al<sub>2</sub>O<sub>3</sub> Cyanamid Ketjen CK 300 and Rodhia HSA5, respectively.

BET surface areas (SA) were measured by N<sub>2</sub> physisorption at its boiling point using an Autosorb Quantachrome 1-C sorptometer. The sample structural properties were determined by X-ray diffraction (XRD) technique using a Shimadzu XD-D1 instrument. The Cu chemical content of the catalyst was analyzed by atomic absorption spectrometry (AAS).

Catalyst base site number (*n*<sub>b</sub>) was measured by temperature-programmed desorption (TPD) of CO<sub>2</sub> preadsorbed at room temperature. Sample was exposed to a flowing mixture of 3% of CO<sub>2</sub> in N<sub>2</sub> until surface saturation. Then, weakly adsorbed CO<sub>2</sub> was removed by flushing with N<sub>2</sub>. Finally, the temperature was increased to 773 K at a ramp rate of 10 K/min. The desorbed CO<sub>2</sub> was converted into CH<sub>4</sub> on a Ni/Kieselghur catalyst at 673 K and then analyzed using a flame ionization detector (FID) [7]. The acid site number (*n*<sub>a</sub>) was determined by TPD of NH<sub>3</sub> preadsorbed at room temperature. Samples were pretreated in He at 773 K for 1 h and then exposed at room temperature to a flow of 1.01% NH<sub>3</sub>/He until surface saturation. Weakly adsorbed NH<sub>3</sub> was removed by flowing 60 cm<sup>3</sup>/min of He, and then the temperature was increased to 773 K at 10 K/min. The NH<sub>3</sub> concentration in the effluent was analyzed by mass spectrometry (MS).

The dispersion of the metallic copper particles (*D*) was measured by two consecutive experiments of temperature programmed reduction (TPR) [16]. In the TPR experiments, a reducing mixture of 5% H<sub>2</sub>/Ar at a flow rate of 50 cm<sup>3</sup>/min was used; the reactor was loaded with a molar amount of copper (150 μmol) [17] so that to meet the criteria of Monti et al. [18] and Malet et al. [19]. A heating rate of 10 K/min from 298 to 653 K was used. A mass spectrometer (MS) in a Baltzers Omnistar unit monitored the hydrogen consumption. Quantitative H<sub>2</sub>-uptakes were calculated by integration of the experimental TPR curves and using a previous calibration curve with CuO powder (Cicarelli, PA). Thus, from the first TPR experiment, Cu<sup>T</sup><sub>TPR</sub> values in g Cu/g cat. were obtained, representing the total amount of reducible copper species up to 653 K. The degree of reduction reached by the sample at 653 K was defined as Cu<sup>t</sup><sub>TPR</sub>/Cu<sup>T</sup><sub>AAS</sub> × 100, where Cu<sup>T</sup><sub>AAS</sub> is the total copper content in the catalyst formulation measured by AAS (Cu<sup>T</sup><sub>AAS</sub> = Z/100). The number of surface metallic copper atoms (Cu<sup>S</sup>) in g Cu/g cat. was determined after sample reduction and surface re-oxidation to Cu<sub>2</sub>O using N<sub>2</sub>O. The N<sub>2</sub>O decomposition conditions (reaction temperature and pulse volume) were carefully chosen to avoid bulk copper oxidation [20]. Samples were exposed to pulses of N<sub>2</sub>O (5 × 10<sup>-3</sup> cm<sup>3</sup>) at 363 K until surface saturation. The stoichiometry of the surface re-oxidation reaction is Cu/N<sub>2</sub>O = 2. N<sub>2</sub>O and evolved N<sub>2</sub> signals were monitored by MS. Then, after flushing with Ar, a second TPR experiment was performed up to 653 K to reduce surface Cu<sub>2</sub>O. Under these reduction conditions bulk copper and surface ceria reduction are kept to a minimum [21]. From the area (A<sup>S</sup>) under the TPR curve, the hydrogen uptake was determined and Cu<sup>S</sup> was calculated considering a stoichiometry of Cu/H<sub>2</sub> = 2 [22,23]. Dispersion was defined as *D* = Cu<sup>S</sup>/Cu<sup>T</sup><sub>AAS</sub> = 200 × A<sup>S</sup> × F × MW<sub>Cu</sub>/Z, where A<sup>S</sup> is the area under the TPR curve in Ampere × s/g cat., F is the calibration factor in mol Cu/(Ampere × s), MW<sub>Cu</sub> is the

molecular weight of Cu in g Cu/mol Cu. The number of exposed Cu<sup>0</sup> species was calculated as  $n_{Cu} (\mu\text{mol/g cat}) = 157 \times D \times Z$  and the average copper particle size as  $L (\text{nm}) = 6000 / (\rho_{Cu} S_{Cu}) = 1.04/D$ , assuming spherical particles, a copper density  $\rho_{Cu} = 8.96 \text{ g/cm}^3$  and a Cu surface density of  $1.47 \times 10^{19} \text{ Cu atoms/m}^2$  [24];  $S_{Cu} (\text{m}^2/\text{g Cu}) = D \times 6.02 \times 10^{23} / (1.47 \times 10^{19} \times MW_{Cu}) = 644$   $D$  stands for the copper surface area.

## 2.2. Catalytic testing

Vapor-phase conversion of 2-hexanol (C6OL) was carried out at 573 K and 101.3 kPa in a fixed-bed reactor at contact times ( $W/F_{C6OL}^0$ ) of 11–500 g cat h/mol of C6OL. Before the catalytic tests, catalysts were pretreated in a flow of N<sub>2</sub> at 773 K for 1 h. Then, the catalyst was reduced in situ in flowing H<sub>2</sub> (35 cm<sup>3</sup>/min) at 573 K for 1 h. C6OL (Aldrich ≥ 98.0%) was introduced via a syringe pump and vaporized into flowing N<sub>2</sub> or H<sub>2</sub> to give a pressure ( $P_{C6OL}$ ) of 4.1 kPa. Reaction products were analyzed by on-line gas chromatography using an Shimadzu GC-2014 chromatograph equipped with flame ionization detector and a (5% Phenyl)-methylpolysiloxane HP-5 Agilent capillary column. Data were collected every 0.5 h for 5 h. Unknown species were identified using a Varian Saturn 2000 GC/MS with a NIST library of spectra. Some heavy and branched species could not be identified using that library. Thus, the atomic mass of the molecular ion fragment was used for their identification. Products are denoted as C6K (2-hexanone), CnK (ketones), CnO (oxygenates), CnH (hydrocarbons) and CnOL (alcohols), where n is the carbon atom number in the molecule. Due to a slight catalyst deactivation process, the catalytic results were calculated by extrapolation of the reactant and product concentration curves to zero time on stream. Then,  $X_{C6O}$ , S and Y represent conversion, selectivity and yield at  $t=0$ , respectively. The equilibrated nature of C6OL–C6K interconversions [25] at the present reaction conditions, allows us to consider these two molecules hereinafter as the reactant pool. Thus, conversion was defined for the reactant pool (C6O = C6OL + C6K) as:

$$X_{C6O} = \left( 1 - \frac{F_{C6OL} + F_{C6K}}{F_{C6OL}^0} \right)$$

where  $F_{C6OL}$  and  $F_{C6K}$  are the molar flow rate of C6OL and C6K, respectively, at the reactor exit;  $F_{C6OL}^0$  is the molar flow rate of C6OL in the reactor feed.

Product selectivity was calculated on a carbon atom basis, as:

$$S_i = \frac{F_i N_i}{\sum_i F_i N_i}$$

where  $N$  is the carbon atom number of product “ $i$ ”. Carbon balances closed to within 4–8%.

Pool turnover rates (TOR) are defined as the moles of C6O converted per mol of Cu<sup>0</sup> surface site and per second. Similarly, site time yield (STY) is defined as the moles of product per mol of Cu<sup>0</sup> surface site and per second.

## 3. Results and discussion

### 3.1. Catalyst characterization

Binary Cu–Mg, Cu–Ce and Cu–Al, and ternary Cu–Mg–Al and Cu–Mg–Ce mixed oxides, were prepared by coprecipitation and characterized by several techniques. Catalysts were denoted as ZCuM<sub>I</sub>(M<sub>II</sub>), where Z represents the copper content in wt.% and M<sub>I</sub> and M<sub>II</sub> are the accompanying cations (Mg<sup>2+</sup>, Al<sup>3+</sup> or Ce<sup>4+</sup>). These cations were selected because of the known acid–base properties of their corresponding single oxides for conversion of alcohols and

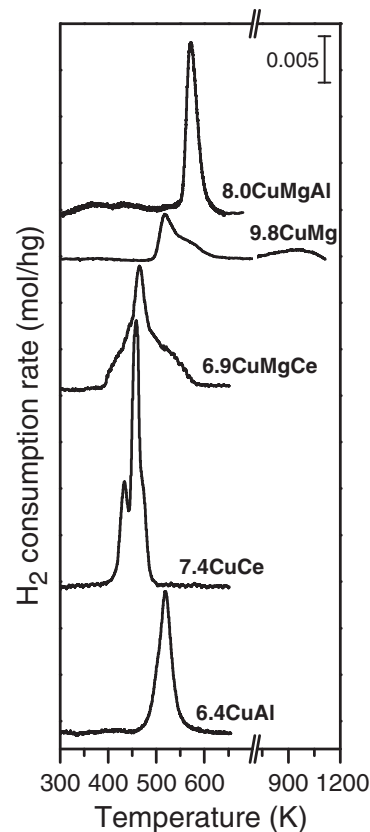


Fig. 1. TPR profiles of ZCuM<sub>I</sub>(M<sub>II</sub>) oxides.

polyols [7,9,26,27]. On the other hand, 9.8CuMg and 6.4CuAl catalysts were prepared to represent typically, bifunctional metal–base or metal–acid catalysts, respectively.

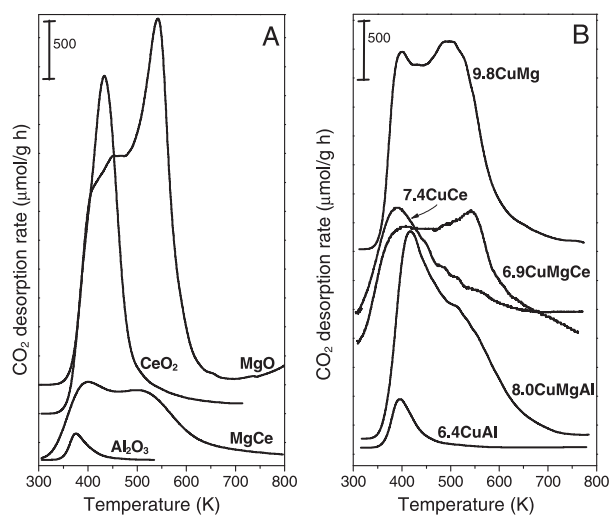
The physicochemical properties of the oxides prepared in this work are summarized in Table 1. Elemental analysis revealed that the measured Cu loadings of about 6–10 wt.% were very close to the nominal values, therefore confirming complete precipitation of the cations during the synthesis procedure [28]. The structural analysis and the identification of the crystalline phases present in the ZCuM<sub>I</sub>(M<sub>II</sub>) oxides were carried out by XRD (diffractograms not shown here). In samples 9.8CuMg, 6.4CuAl and 8.0CuMgAl, no crystalline copper species was detected and they only showed the single quasi-amorphous MgO or γ-Al<sub>2</sub>O<sub>3</sub> phase. Partial incorporation of Al<sup>3+</sup> cations in the MgO matrix of sample 8.0CuMgAl was inferred by calculations of the MgO lattice parameter ( $a_{MgO}$ ), Table 1. The contraction of the MgO unit cell in the 8.0CuMgAl oxide (4.150 Å) compared with that of pure MgO (4.216 Å) is the result of substitution of smaller Al<sup>3+</sup> cations ( $r_{Al^{3+}} = 0.535 \text{ \AA}$ ) for Mg<sup>2+</sup> ( $r_{Mg^{2+}} = 0.72 \text{ \AA}$ ) in the structure. An incipient CuO phase (tenorite) was detected in 7.4CuCe and 6.9CuMgCe samples.

The fact that copper species were hardly detected in the ZCuM<sub>I</sub>(M<sub>II</sub>) samples indicates that these species are either highly dispersed as small CuO crystallites not detectable by XRD or forming a solid solution within the oxide lattice. To get insight into this issue, the reducibility of Cu species in ZCuM<sub>I</sub>(M<sub>II</sub>) samples was investigated by TPR. Fig. 1 shows the reduction profiles obtained after sample calcination in air at 773 K. Quantification of the reduced copper species was carried out considering that the observed H<sub>2</sub> consumption peaks of Fig. 1 correspond to Cu<sup>2+</sup> → Cu<sup>0</sup> reduction [29]. The dispersion ( $D$ ) values were comparable to those reported for comparable Cu-based oxides [8,10,30,31].

The 8.0CuMgAl sample reduced giving a single and broad reduction peak at around 550–650 K with a temperature at peak

**Table 1**  
Physicochemical properties of ZCuM<sub>I</sub>(M<sub>II</sub>) catalysts and Cu-free oxides.

Catalyst	Surface area, SA (m <sup>2</sup> /g)	Nominal composition (wt.%)			Structural analysis by XRD			Cu species reducibility, dispersion and size			Acid-base properties (μmol/g)		
		Cu	Mg	Al	Ce	$a_{\text{MgO}}$ <sup>a</sup> (Å)	Phases detected	D <sup>b</sup> (%)	$n_{\text{Cu}}$ <sup>c</sup> (μmol/g)	L <sup>d</sup> (nm)	$T_M$ <sup>e</sup> (K)		
9.8CuMg	198	10.0	53.1	—	—	4.251	MgO	2.7	42	12.4 <sup>f</sup>	518	652	20
8.0CuMgAl	248	7.8	29.7	21.4	—	4.150	MgO	12.2	154	8.5	571	457	124
6.9CuMgCe	102	7.7	29.4	—	33.9	4.213	CeO <sub>2</sub> –CuO–MgO	7.0	76	14.9	464	275	30
7.4CuCe	74	7.8	—	—	73.5	—	CeO <sub>2</sub> –CuO	14.0	163	7.4	458	170	74
7.4CuAl	211	7.1	—	48.2	—	—	γ-alumina	13.9	140	7.5	518	45	253
MgO	189	—	—	60.3	—	—	MgO	—	—	—	—	655	15
CeO <sub>2</sub>	260	—	—	—	—	—	CeO <sub>2</sub>	—	—	—	—	354	42
MgCe	103	—	—	32.4	—	—	CeO <sub>2</sub> –MgO	—	—	—	—	247	15
Al <sub>2</sub> O <sub>3</sub>	230	—	—	—	52.9	—	γ-alumina	—	—	—	—	19	186

<sup>a</sup> MgO lattice constant.<sup>b</sup> Cu<sup>0</sup> dispersion by N<sub>2</sub>O decomposition.<sup>c</sup> Number of exposed Cu<sup>0</sup> species.<sup>d</sup> Cu<sup>0</sup> particle size.<sup>e</sup> Temperature at peak maximum by TPR.<sup>f</sup> Calculated from the dispersion of reducible particles using sample degree of reduction (see Section 2.1).<sup>g</sup> Base site number by TPD of CO<sub>2</sub>.<sup>h</sup> Acid site number by TPD of NH<sub>3</sub>.

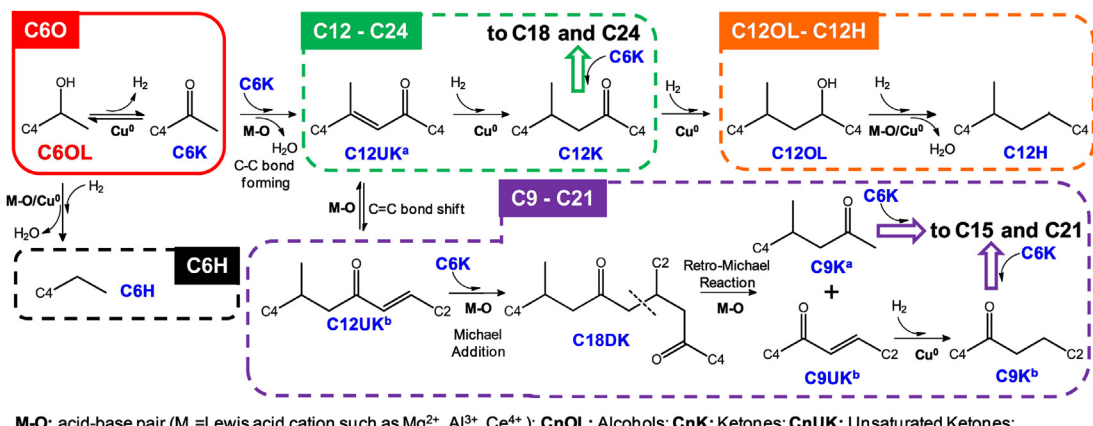
**Fig. 2.** TPD of CO<sub>2</sub> for (A): copper-free oxides; (B): ZCuM<sub>I</sub>(M<sub>II</sub>) oxides.

maximum ( $T_M$ ) of 571 K; quantitative TPR analysis indicated that total reduction was achieved below 653 K. Similarly, sample 6.4CuAl showed also stoichiometric reduction below 653 K, giving a broad peak with a  $T_M$  value of 518 K, very close to that of pure reference CuO (502 K) [10]. In addition, these two samples showed similar  $D$  values, of around 12–14% (Table 1). Contrarily, in sample 9.8CuMg just 33% of the total copper atoms were reduced below 653 K and complete reduction was reached just at 1100 K. Thus, it seems that in 9.8CuMg, part of the Cu<sup>2+</sup> ions form a Cu–Mg solid solution in which Cu species are more difficult to reduce. As a result, the Cu<sup>0</sup> dispersion in sample 9.8CuMg (2.7%, Table 1) was much lower than in the other samples.

Formation of a Cu–Mg solid solution in sample 9.8CuMg is supported by the values of the  $a_{\text{MgO}}$  parameter reported in Table 1. In fact, since the ionic radius of octahedrally coordinated Cu<sup>2+</sup> ( $r_{\text{Cu}^{2+}} = 0.73 \text{ Å}$ ) is slightly larger than that of Mg<sup>2+</sup> in MgO [32], the small expansion of the MgO lattice (higher  $a_{\text{MgO}}$  values) would result from the substitution of small amounts of Cu<sup>2+</sup> for Mg<sup>2+</sup> ions within the MgO structure. Solubility of the Cu<sup>2+</sup> ions within the MgO structure is favored by the slight difference in ionic size between Cu<sup>2+</sup> and Mg<sup>2+</sup>.

On the other hand, 6.9CuMgCe and 7.4CuCe reduced at lower temperatures than the other ZCuM<sub>I</sub>(M<sub>II</sub>) samples giving a sharp peak with a  $T_M$  of ~460 K. It has been reported that the Cu reducibility enhancement in Cu–Ce mixed oxides is due to weakening of the Cu–O bond [33]. The degree of reduction was above 100% on these samples what means that the hydrogen consumption exceeded in 14–16% the amount needed to completely reduce Cu<sup>2+</sup> to Cu<sup>0</sup> species. Although there is no general agreement in the literature concerning the interpretation and assignment of the hydrogen consumption peaks, two phenomena might account for the surplus TPR area: a partial surface reduction of ceria at ~373–423 K and a hydrogen adsorption on the ceria surface [21,34,35]. The latter effect has no influence on the dispersion calculation. Contrarily, partial reduction of CeO<sub>2</sub> might lead to an overestimation of the copper dispersion. Nevertheless, under the present conditions for dispersion calculations ceria reduction is expected to be below 10% [21].

The surface basic properties of the ZCuM<sub>I</sub>(M<sub>II</sub>), MgO, CeO<sub>2</sub>, MgCe and Al<sub>2</sub>O<sub>3</sub> catalysts were investigated by TPD of CO<sub>2</sub>, Fig. 2. The number of base sites ( $n_b$ , μmol/g) was calculated by integration of the TPD curves and results are shown in Table 1. Similar to pure MgO (Fig. 2A), the Mg-containing samples (8.0CuMgAl, 6.9CuMgCe and 9.8CuMg) of Fig. 2B desorb CO<sub>2</sub> in a wide temperature range of 350–700 K, reflecting the presence of surface sites that



**Scheme 1.** Reaction steps for the conversion of C6OL on bifunctional metal-base catalysts.

adsorb  $CO_2$  with different binding energies. The shape of the TPD curves, that indicates the base strength distribution, depends on the Mg and Al content, Table 1. The presence of increasing amounts of acidic  $Al^{3+}$  cations in the formulation of  $ZCuM_I(M_{II})$  samples shifts the peak maximum to lower temperatures and decreases the total number of base sites compared to 9.8CuMg. Thus, 6.4CuAl presents less and weaker base sites than other  $ZCuM_I(M_{II})$  samples. In the Ce-containing samples (6.9CuMgCe and 7.4CuCe) the effect of increasing the  $Ce^{4+}$  content is similar to that of  $Al^{3+}$  because both cations are more electronegative than  $Mg^{2+}$  [36].

In addition, the number of acid sites ( $n_a$ ,  $\mu\text{mol/g}$ ) was measured on the  $ZCuM_I(M_{II})$  catalysts and on the Cu-free oxides by TPD of  $NH_3$  (Table 1). Alumina, and Al-containing samples (6.4CuAl, 8.0CuMgAl) exhibited the highest  $n_a$  values. All the other single or mixed oxides presented a low number of surface acid sites.

### 3.2. Role of base, acid and metallic copper sites in the catalytic performance of $ZCuM_I(M_{II})$ catalysts

The gas-phase conversion of C6OL into heavier compounds was studied on the  $ZCuM_I(M_{II})$  catalysts. The products of the reaction were C3–C24 oxygenates and hydrocarbons. Formation of short chain compounds such as C3O and C3H by C–C bond cleavage and of C6H by C6OL dehydration is undesirable. In fact, the synthesis of compounds to be used as liquid transportation fuels involves the C–C bond forming aldol condensation reaction as part of a series of consecutive reaction steps that comprises dehydrogenation, C–C

coupling, dehydration and hydrogenation reactions (Scheme 1). The sequence depicted in Scheme 1 starts by the dehydrogenation of C6OL to C6K (block C6O), but alcohols such as C6OL may also dehydrate to C6H (block C6H), on  $ZCuM_I(M_{II})$  catalysts [10]. Then, selective C6OL conversion to C6K may be challenging because  $ZCuM_I(M_{II})$  catalysts must contain some dehydrating properties in order to promote the dehydration steps involved in the formation of higher C12–C24 compounds. Moreover, Cu was chosen because it preferentially activates the O–H bond of alcohols, giving aldehydes or ketones by dehydrogenation at mild temperatures without significantly breaking the C–C bonds. On the other hand, the right selection of the base sites is a trade-off process between the need of basic properties to promote the aldol condensation steps and the detrimental base-catalyzed C–C bond cleavage reactions leading to light compounds [26].

The role of base and  $Cu^0$  sites in the synthesis of C9–C24 compounds from the reactant pool, C6O = C6OL + C6K, was investigated by testing the different  $ZCuM_I(M_{II})$  catalysts and the reference copper-free  $MgO$ ,  $CeO_2$ ,  $MgCe$  and  $Al_2O_3$  samples at 573 K. The C6O conversion ( $r_{C6O}$ ) and turnover (TOR) rates are shown in Table 2. The selectivity to C3 ( $S_{C3O-C3H}$ ), C6H ( $S_{C6H}$ ) and C9–C24 compounds ( $S_{C9-C24}$ ) at 20% conversion are also included in Table 2.

Time ago, we investigated the participation of basic sites in the coupling reactions of primary and secondary alcohols [7,28,37] on Mg-Al mixed oxides with different Mg/Al ratios. We demonstrated that the complex reaction pathways involved in aldol condensation reactions require specific combinations of acid and base sites, i.e.,

**Table 2**

Activity and selectivity of  $ZCuM_I(M_{II})$  catalysts and Cu-free oxides.

Catalyst	Catalytic results						
	$r_{C6O}^a$ (mmol/hg)	TOR <sup>b</sup> ( $s^{-1}$ ) × 100	$S_{C3O-C3H}^c$ (%)	$S_{C6H}^c$ (%)	$S_{C9-C24}^c$ (%)	$S_{CnO}/S_{CnH}^d$ n = 9–24	O/C <sup>e</sup> n = 9–24
9.8CuMg	1.96	1.31	3.0	0.8	96.2	6.50	0.074
8.0CuMgAl	8.42	1.52	3.3	1.7	95.0	8.04	0.067
6.9CuMgCe	1.93	0.70	2.1	1.3	96.6	7.94	0.076
7.4CuCe	6.10	1.04	0.6	79.9	19.5	0.83	0.043
6.4CuAl	367.97	73.01	0.1	99.9	0.0	–	–
MgO	0.53	–	0.3	64.1	35.6	1.71	0.053
CeO <sub>2</sub>	4.47	–	2.2	89.9	7.9	1.18	0.047
MgCe	1.10	–	1.2	78.3	20.5	1.68	0.053
Al <sub>2</sub> O <sub>3</sub>	165.16	–	0.1	99.9	0.0	–	–

<sup>a</sup> Reaction rate.

<sup>b</sup> Turnover rate per mol surface  $Cu^0$  site.

<sup>c</sup> Selectivity at  $X_{C6O} = 20\%$ .

<sup>d</sup> Oxygenates/hydrocarbons selectivity ratio for C9–C24 compounds at  $X_{C6O} = 20\%$ .

<sup>e</sup> Atom ratio in the C9–C24 product pool at  $X_{C6O} = 20\%$ .

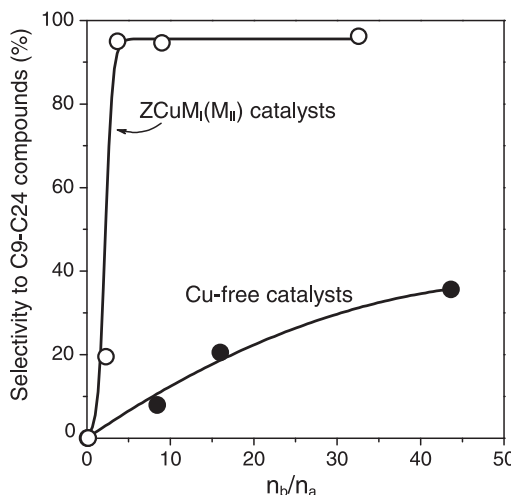


**Fig. 3.** Selectivity to C9–C24 products on copper-free and ZCuM<sub>I</sub>(M<sub>II</sub>) oxides as a function of the base/acid site ratio,  $n_b/n_a$ . [T = 573 K, P = 101.3 kPa,  $\bar{P}_{C6OL}$  = 4.1 kPa,  $X_{C6O}$  = 20%].

an adequate balance between Mg<sup>2+</sup> and Al<sup>3+</sup> cations. The active site is a M<sup>n+</sup>–O<sup>2-</sup> pair (M = Lewis acid cation) with moderate basic properties. Thus, strongly basic pure MgO was in general less active than the Mg-rich Mg-Al oxides with milder basic properties. On the other hand, alumina was much more active than any Mg-Al oxide, but the products were olefins and ethers formed by alcohol dehydration.

Here, we show in Table 2 that alumina readily dehydrates C6OL to C6 hydrocarbons (hexane and hexene, C6H), reflecting its high surface acidity (Table 1). No C9–C24 condensation products were detected on this sample in line with their poor basic properties shown in Table 1 and Fig. 2A. On the other hand, pure MgO shows low activity for converting C6O but forms significant amounts of C9–C24 compounds resulting from coupling reactions. In line with their acid–base properties, the activity and product distribution on CeO<sub>2</sub> and MgCe oxides are halfway between those on Al<sub>2</sub>O<sub>3</sub> and MgO. In this regard, the plot of the selectivity toward C9–C24 compounds as a function of the base/acid site ratio ( $n_b/n_a$ ) in Fig. 3 clearly shows that  $S_{C9-C24}$  increases with increasing  $n_b/n_a$  values on Cu-free samples.

Similarly to alumina, 6.4CuAl dehydrates C6OL at high rates without yielding any C9–C24 products because the Al<sup>3+</sup>–O<sup>2-</sup> pairs are not basic enough to promote C–C bond forming reactions. Thus, hexane (C6H) is the main product on 6.4CuAl (hexene or other olefins were never observed on Cu-containing catalysts). In contrast, 9.8CuMg, 6.9CuMgCe and 8.0CuMgAl contain a high concentration of strong base sites (Mg<sup>2+</sup>–O<sup>2-</sup> pairs, Fig. 2B) that almost completely suppress the dehydrating activity toward C6H.

Thus, selectivity toward C9–C24 compounds is more than 95% on these Mg-containing samples. Sample 7.4CuCe, which contains weakly basic Ce<sup>4+</sup>–O<sup>2-</sup> sites (Fig. 2B), forms only 19.5% of C9–C24 aldol condensation products. Fig. 3 presents the evolution of  $S_{C9-C24}$  as a function of  $n_b/n_a$  ratio on Cu-containing samples and shows that besides the effect of the catalyst acid–base properties, the presence or not of dispersed Cu<sup>0</sup> species in the catalyst formulation has a marked influence on the selectivity toward C9–C24 compounds.

Bifunctional metal–base catalysts such as 9.8CuMg, 6.9CuMgCe and 8.0CuMgAl are more active and selective to C9–C24 compounds than MgO (Table 2), despite their weaker basicity (Table 1 and Fig. 2). In addition, bifunctional metal–acid catalyst 6.4CuAl is more active than its homologous Al<sub>2</sub>O<sub>3</sub> in spite of the fact that both samples present comparable acidic properties. Similar activity increase can be observed by comparing CeO<sub>2</sub> with 7.4CuCe and

MgCe with 6.9CuMgCe. Thus, the superior catalytic performance of bifunctional catalysts may be attributed to the ability of surface Cu<sup>0</sup> species to promote the initial reaction step, i.e., the C6OL dehydrogenation or dehydration, by activating the alcohol O–H or C–O bonds, respectively. Similarly, we expect here that because of the presence of dispersed Cu<sup>0</sup> particles, the surface coverage of C6K species that initiate the aldol condensation sequence (block C6O, Scheme 1) be substantially higher on the bifunctional metal–base catalysts than on pure MgO. That explains the higher selectivity to C9–C24 aldol condensation products obtained on bifunctional catalysts.

Table 2 also shows the oxygenates/hydrocarbons ( $S_{CnO}/S_{CnH}$ ) selectivity ratio for C9–C24 compounds at 20% conversion. The higher  $S_{CnO}/S_{CnH}$  values obtained on the bifunctional metal–base catalysts compared to their Cu-free homologues, is the result of the higher surface coverage of oxygenate species formed by C–C coupling reactions (mainly C12O) and hydrogen fragments originated from the initial C6OL dehydrogenation. Scheme 1 shows that hydrogen is needed after the aldol condensation step to further proceed with the reaction sequence leading to formation of alcohols and finally, hydrocarbons.

The O/C atom ratio is 0.8 in cellulose [38], 1.0 in monosaccharide sugars, and 0.167 in the reactant C6OL. Table 2 shows that the calculated O/C atom ratio in the C9–C24 product pool obtained on ZCuM<sub>I</sub>(M<sub>II</sub>) catalysts was more than 60% smaller than in C6OL. This result indicates that the strategy chosen here for upgrading of C6OL gives a product mixture with superior hydrophobic properties than C6OL.

The values of C6OL conversion rate per Cu metal site (turnover rate, TOR) and of site time yield (STY) for formation of the most relevant products obtained on Cu-containing catalysts are presented in Table 2 and Fig. 4. In Fig. 4A, the TOR values are plotted as a function of the number of base sites,  $n_b$ . The highest TOR value was obtained on the bifunctional metal–acid 6.4CuAl catalyst with negligible basicity. TOR then decreases with  $n_b$ , goes through a minimum and finally reaches a constant value for the metal–base catalysts with the highest  $n_b$ . The shape of the TOR vs  $n_b$  curve in Fig. 4A suggests that the rate-limiting step changes as  $n_b$  increases and that on catalysts with  $n_b > 400 \mu\text{mol/g}$  the reaction is controlled by similar rate-limiting steps. Fig. 4B shows the evolution of STY for formation of C3, C6H and C9–C24 compounds as a function of  $n_b$ . The STY for C9–C24 aldol condensation products (open squares in Fig. 4B) increases with  $n_b$  up to  $n_b \leq 400 \mu\text{mol/g}$  and then remains approximately constant. This suggests that for  $n_b < 400 \mu\text{mol/g}$ , the rate-limiting step of the bifunctional process leading to C9–C24 products is the base-catalyzed C–C bond forming reaction. On the other hand, the fact that samples 8.0CuMgAl and 9.8CuMg ( $n_b > 400 \mu\text{mol/g}$ ) exhibit similar STY values for C9–C24 compound formation seems to indicate that on these catalysts the process is limited by the Cu-promoted hydrogenation steps. Thus, participation of surface Cu<sup>0</sup> species or M<sup>n+</sup>–O<sup>2-</sup> pairs in the rate-limiting steps of aldol condensation product formation depends on the relative abundance of these sites in the bifunctional catalysts.

Scheme 1 summarizes the role played in the reaction sequence by both surface active species: the metallic Cu<sup>0</sup> particles and the Lewis acid cation–oxygen anion pair site.

### 3.3. Effect of the reaction atmosphere and contact time. Reaction pathways

The catalytic results of the previous section show that 8.0CuMgAl is the most promising bifunctional metal–base catalyst for C6OL conversion into C9–C24 aldol condensation products. This catalyst combines a high Cu<sup>0</sup> dispersion with moderate basic properties; base sites are expected to be surface oxygen species in Mg<sup>2+</sup>–O<sup>2-</sup> pairs. These pairs are located in a particular chemical

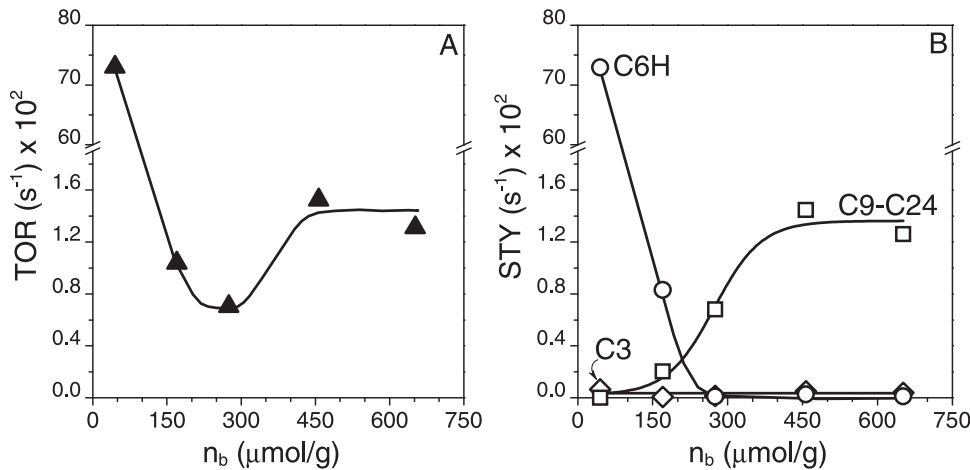


**Fig. 4.** (A) Turnover rate, TOR, and (B) Site time yield, STY, for C3, C6H and C9–C24 products as a function of the number of base sites,  $n_b$ , in ZCuM<sub>I</sub>(M<sub>II</sub>) catalysts [T = 573 K, P = 101.3 kPa,  $\bar{P}_{C6OL}$  = 4.1 kPa].

environment of the oxide matrix where they are surrounded by Al<sup>3+</sup> cations.

Product formation on catalyst 8.0CuMgAl was further studied by changing the contact time and the reaction atmosphere. Fig. 5A shows the conversion of the C6O reactant pool as a function of contact time ( $W/F_{C6OL}^0$ ) on 8.0CuMgAl when the reaction is carried out in N<sub>2</sub> and H<sub>2</sub>. Clearly, the catalyst activity was much higher in H<sub>2</sub>, showing that total conversion was achieved at  $W/F_{C6OL}^0$  = 100 gh/mol, whereas in N<sub>2</sub> the highest conversion was 91% at  $W/F_{C6OL}^0$  = 350 gh/mol and could not be further increased. From the slopes of the curves of Fig. 5A at  $W/F_{C6OL}^0 \rightarrow 0$ , we determined the initial reaction rates ( $r_{C6O}^0$ , mmol/hg); the  $r_{C6O}^0$  value obtained in H<sub>2</sub> (25.8 mmol/hg) was clearly higher than in N<sub>2</sub> (9.6 mmol/hg). From this result, participation of hydrogen in the overall kinetic rate expression is inferred.

The yield to C9–C24 products on 8.0CuMgAl is also higher in H<sub>2</sub> than in N<sub>2</sub>, as shown in Fig. 5B; at the highest conversions of Fig. 5A, 91% of C9–C24 products was quantified in H<sub>2</sub> in contrast to 73% in N<sub>2</sub>. This result confirms the conclusions of the previous section on that the rate-limiting step of the aldol condensation process on the 8.0CuMgAl bifunctional metal–base catalyst is a hydrogenation reaction promoted by Cu<sup>0</sup> species.

The effect of the reaction atmosphere and contact time on the distribution of C9–C24 products was also investigated on catalyst 8.0CuMgAl. Fig. 6 presents the yields of C9 to C24 products (without discriminating between oxygenates and hydrocarbons) as a function of the C6O conversion for the reactions carried out

in N<sub>2</sub> and H<sub>2</sub>. Qualitatively, the product distribution is similar in both reaction atmospheres; at the highest C6O conversions, 53–60% of the products were C9–C12 compounds. However, whereas C12 was the main product in H<sub>2</sub>, C12 and C9 were obtained in similar amounts in N<sub>2</sub>, as will be discussed below. Apart from C12 and C9 compounds, C15 and C18 oxygenates and hydrocarbons were quantified, as well as minor amounts of C21 and C24 products. The non-zero initial slope (at  $X_{C6O} \rightarrow 0$ ) of the C12 yield curve in Fig. 6 is consistent with the direct C12 formation from C6K via the first aldol condensation sequence (formation of C12UK<sup>a</sup>, C12K, C12OL and C12H in Scheme 1). At higher conversion levels, the C12 yield curves tend to level off because of consecutive transformation in other compounds (Scheme 1). The zero initial slope of the C18 and C24 yield curves confirm that they are secondary products formed by additional aldol condensation sequences.

The results obtained in the catalytic experiments performed at different atmospheres and  $W/F_{C6OL}^0$  allow us to postulate the reaction network depicted in Scheme 1 for the upgrading of 2-hexanol on ZCuM<sub>I</sub>(M<sub>II</sub>) catalysts. Initially, C6OL is dehydrogenated on Cu metallic sites forming C6K. Then, the C–C bond forming aldol condensation of C6K on Mg<sup>2+</sup>–O<sup>2-</sup> pairs forms an aldol adduct (a hydroxyketone not shown) that is easily dehydrated to the  $\alpha,\beta$ -unsaturated ketone C12UK<sup>a</sup> which in turn can be hydrogenated to saturated C12K. Consecutive hydrogenation steps convert C12K in an alcohol (C12OL) and a hydrocarbon (C12H). The carbon chain can be lengthened further by reaction of C12K with a new C6K molecule

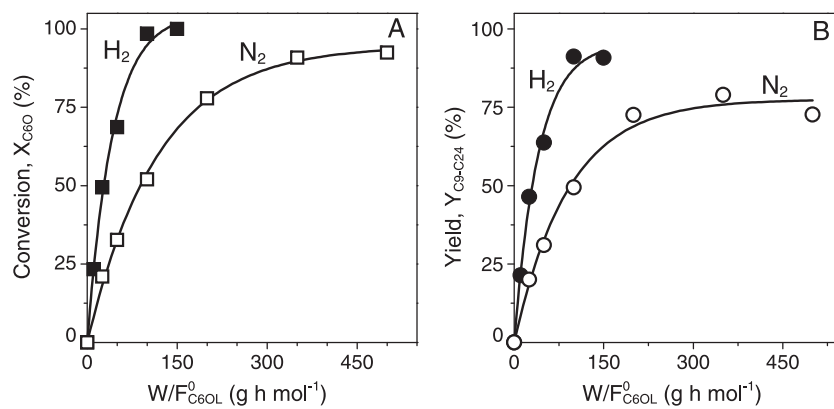


**Fig. 5.** Effect of the reaction atmosphere (N<sub>2</sub> or H<sub>2</sub>) and contact time ( $W/F_{C6OL}^0$ ) on (A): conversion; (B) total yield to C9–C24 products [Catalyst: 8.0CuMgAl, T = 573 K, P = 101.3 kPa,  $\bar{P}_{C6OL}$  = 4.1 kPa].

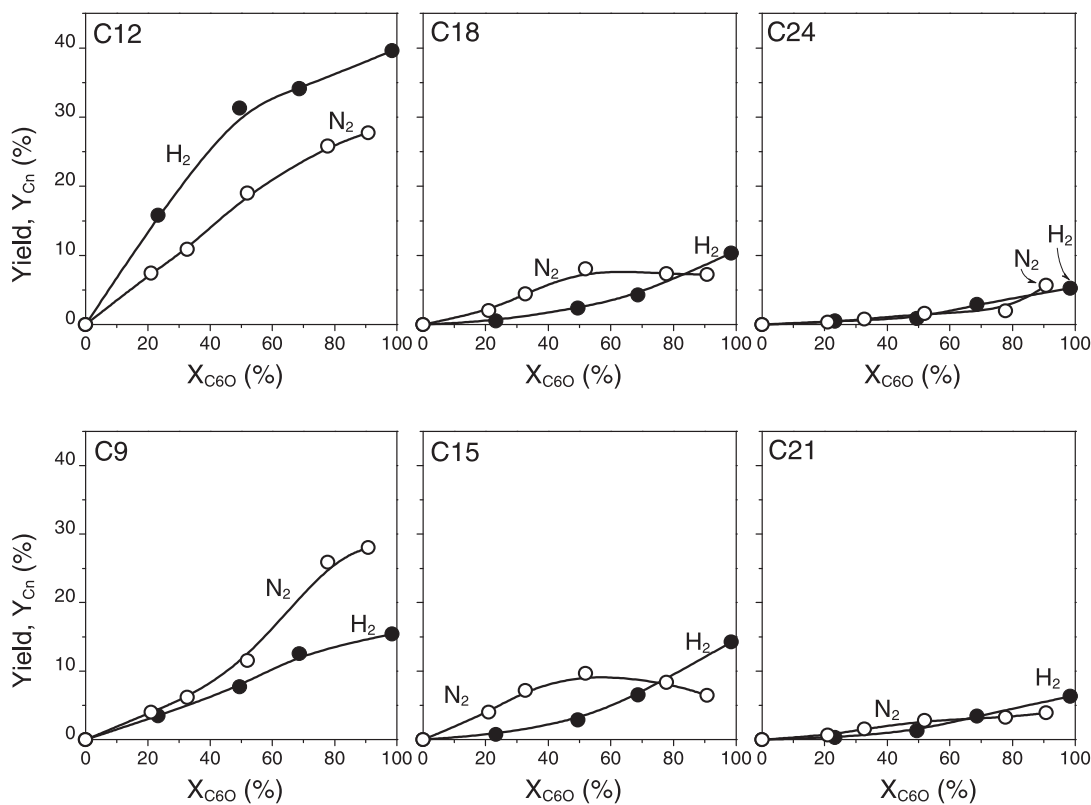
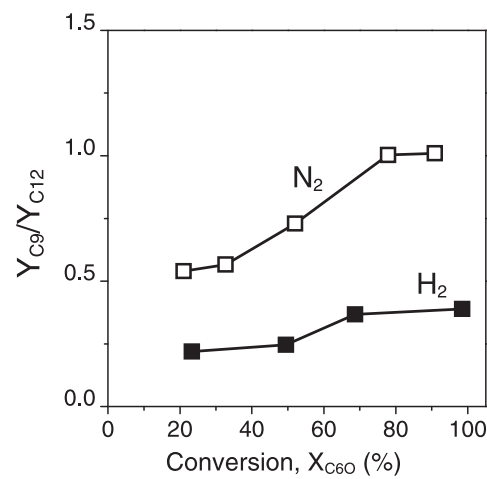


**Fig. 6.** Effect of the reaction atmosphere (N<sub>2</sub> or H<sub>2</sub>). Yield toward C<sub>n</sub> products ( $n=9, 12, 15, 18, 21$  and 24) as a function of conversion [Catalyst: 8.0CuMgAl,  $T=573$  K,  $P=101.3$  kPa,  $\bar{P}_{\text{C6OL}}=4.1$  kPa].

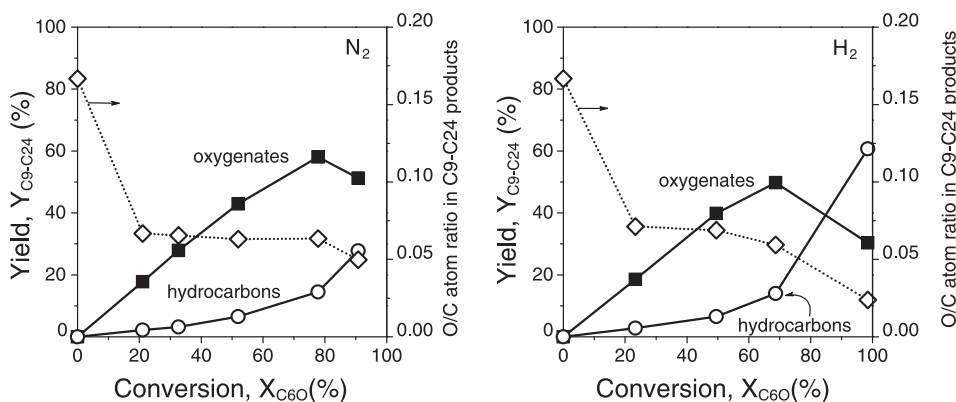
to give ketones, alcohols and hydrocarbons with an even number of carbon atoms, such as C18 and C24.

Fig. 6 shows that significant amounts of products with an odd number of carbon atoms (C9, C15 and C21) are formed from C6OL. However, formation of these compounds is not explained by the reaction sequence described above. The shape of the C9 yield curve in Fig. 6 indicates that C9 are secondary products formed from C12 compounds. In this regard, we recently showed that bifunctional metal-base catalysts such as 8.0CuMgAl promote the C=C bond cleavage of polyols giving rise to lighter oxygenates [10]. However, results of Table 2 and Fig. 4 show selectivities toward C3 products lower than 10%. Thus, the concentration of C3 compounds formed probably by retro-aldol like reactions is not enough to give high yields of C9 products (Fig. 6) by aldol condensation with C6K. This indicates that a different reaction pathway must be applying for formation of products with an odd number of carbon atoms (C9, C15 and C21). Kunkes et al. [25] reported similar results for conversion of hexanone on a Pd/CeZrO<sub>x</sub> catalyst and postulated an alternative pathway for the formation of C9 ketones, depicted as the C9–C21 block of Scheme 1. Initially, the reaction would proceed by the C=C bond shift in the  $\alpha,\beta$ -unsaturated ketone C12UK<sup>a</sup> giving C12UK<sup>b</sup>. Although we did not detect any unsaturated ketone among the reaction products on 8.0CuMgAl, it has to be remarked that in previous works we reported that on similar bifunctional metal-base catalysts, and in the absence of molecular hydrogen,  $\alpha,\beta$ -unsaturated ketones are unstable reaction intermediates that rapidly convert into other products; the C=C bond migration is fast and occurs on base sites before the C=C bond reduction on a metallic site [9,39,40]. In other words, the base-catalyzed C=C bond shift of C12UK<sup>a</sup> would take place faster than the Cu<sup>0</sup>-promoted C=C bond hydrogenation. Formation of C9K continues then by consecutive Michael and retro-Michael reactions, after which conventional aldol condensation steps lead to C15 and C21 products.

The reaction network postulated for C9K formation explains why for the C6OL conversion in N<sub>2</sub>, the yield to C9 products is higher than those to C18 and C24 (Fig. 6). In fact, Fig. 7 shows the C9/C12 yield ratio for the reactions carried out in N<sub>2</sub> and H<sub>2</sub>. The C9/C12 ratio in H<sub>2</sub> is  $\sim 0.3$ , almost independent of the conversion level. This result suggests that in the presence of molecular H<sub>2</sub> the C=C bond of C12UK<sup>a</sup> is rapidly reduced on the Cu<sup>0</sup> sites forming the saturated ketone C12K, which hampers the formation of C9 compounds via the C=C bond shift of C12UK<sup>a</sup>. In contrast, when the reaction is carried out in N<sub>2</sub>, the C9/C12 ratio increases with C6OL conversion, reaching  $\sim 1$  at high conversion levels. In N<sub>2</sub>, the catalyst surface is



**Fig. 7.** Effect of the reaction atmosphere (N<sub>2</sub> or H<sub>2</sub>). C9/C12 yield ratio as a function of conversion [Catalyst: 8.0CuMgAl,  $T=573$  K,  $P=101.3$  kPa,  $\bar{P}_{\text{C6OL}}=4.1$  kPa].



**Fig. 8.** Effect of the reaction atmosphere ( $N_2$  or  $H_2$ ). Yield to oxygenates and hydrocarbons and O/C atom ratio in C9–C24 products as a function of conversion [Catalyst: 8.0CuMgAl,  $T=573\text{ K}$ ,  $P=101.3\text{ kPa}$ ,  $\bar{P}_{\text{C}6\text{OL}}=4.1\text{ kPa}$ ].

deprived of hydrogen (the only source of  $H_2$  in the reaction comes from the initial C6OL dehydrogenation to C6K) which enables the competing C=C bond migration route and explains the much higher C9/C12 ratio.

Finally, we remark that the use of inert or reducing reaction atmospheres ( $N_2$  or  $H_2$ ) affects not only the average molecular weight of the product pool but also the oxygenate content. Fig. 8 presents the yield to C9–C24 oxygenates and hydrocarbons as a function of conversion. The shape of the curves is consistent with hydrocarbons being secondary products formed consecutively to oxygenates, as postulated in Scheme 1. When the reaction is performed in  $N_2$  and only surface-generated hydrogen is available for hydrogenation of oxygenates, the latter are the dominant products. Oxygenates also predominate when  $H_2$  is fed to the reactor, but their hydrogenation to hydrocarbons occurs much faster than in  $N_2$  so that they are the main products at high conversions. Fig. 8 also shows that the O/C atom ratio in the C9–C24 product pool can be notoriously decreased compared to that of C6OL (0.167). The effect of  $H_2$  on that ratio is also evident since at the highest conversions, the O/C value in  $H_2$  (0.024) is half of that in  $N_2$  (0.05).

#### 4. Conclusions

Bifunctional metal-base Cu–M<sub>I</sub>–M<sub>II</sub> mixed oxides (M<sub>I</sub>, M<sub>II</sub>: Mg<sup>2+</sup>, Al<sup>3+</sup>, Ce<sup>4+</sup>) are active and selective catalysts to transform 2-hexanol in C9–C24 oxygenates and hydrocarbons with applications as liquid transportation fuels. Formation of these compounds occurs by tandem dehydrogenation, C–C bond formation, dehydration and hydrogenation reactions.

Well dispersed metallic Cu<sup>0</sup> particles promote dehydrogenation and hydrogenation steps whereas moderately basic acid–base sites provided by M<sub>I</sub>(M<sub>II</sub>)–O pairs participate in the C–C coupling by aldol condensation. Hydrogenation is the rate-limiting step for C9–C24 formation on catalysts with a high number of base sites. However, the shift of the rate-limiting step to the C–C bond formation reaction occurs on catalysts with lower relative abundance of base sites.

The most promising catalyst is a Cu–Mg–Al mixed oxide with 8 wt.% Cu that yields 73–91% C9–C24 compounds, depending on the operating conditions under inert or reducing atmosphere. The C9–C24 product pool is a hydrophobic mixture of monofunctional compounds with one or none oxygen atom, in which the O/C atom ratio is as low as 0.024 and consists of branched alcohols, ketones and alkanes. More than 50% of the C9–C24 products are in the mass range of C9–C12.

Products with odd carbon atom number are formed through a distinct reaction pathway compared to products with even carbon atom number. The availability of hydrogen atoms determines

which pathway predominates, so that C9, C15 and C21 products are more likely formed under inert atmospheres.

#### Acknowledgements

Authors thank the Agencia Nacional de Promoción Científica y Tecnológica (ANPCyT), Argentina (grant PICT 1888/10), the CONICET, Argentina (grant PIP 11220090100203/10) and Universidad Nacional del Litoral, Santa Fe, Argentina (grant CAID PI 64–103/11) for financial support of this work.

#### References

- [1] A. Corma, S. Iborra, A. Velty, Chem. Rev. 107 (2007) 2411.
- [2] J.Q. Bond, D.M. Alonso, J.A. Dumesic, in: E. Wyman (Ed.), Chapter 5 in "Aqueous Pretreatment of Plant Biomass for Biological and Chemical Conversion to Fuels and Chemicals", 1st ed., John Wiley & Sons, 2013, ISBN: 9780470972021.
- [3] J.N. Chheda, J.A. Dumesic, Catal. Today 123 (2007) 59–70.
- [4] J.C. Serrano-Ruiz, J.A. Dumesic, Energy Environ. Sci. 4 (2011) 83–99.
- [5] D.A. Simonetti, J.A. Dumesic, ChemSusChem 1 (2008) 725–733.
- [6] E.L. Kunke, D.A. Simonetti, R.M. West, J.C. Serrano-Ruiz, C.A. Gärtner, J.A. Dumesic, Science 322 (2008) 417.
- [7] J.I. Di Cosimo, G. Torres, C.R. Apesteguía, J. Catal. 208 (2002) 114–123.
- [8] G. Torres, C.R. Apesteguía, J.I. Di Cosimo, Appl. Catal. A: Gen. 317 (2007) 161–170.
- [9] J.I. Di Cosimo, A. Acosta, C.R. Apesteguía, J. Mol. Catal. A: Chem. 222 (2004) 87–96.
- [10] P.A. Torresi, V.K. Díez, P.J. Luggren, J.I. Di Cosimo, Catal. Sci. Technol. 4 (2014) 3203–3213.
- [11] J.J. Bravo-Suarez, B. Subramaniam, R.V. Chaudhari, Appl. Catal. A: Gen. 455 (2013) 234–246.
- [12] M. Zhou, Z. Feng, H. Zhu, G. Xiao, R. Xia, J. Energy Chem. 23 (2014) 91–96.
- [13] S. Tanasoi, N. Tanchoux, A. Urda, D. Tichit, I. Sandulescu, F. Fajula, I.-C. Marcu, Appl. Catal. A: Gen. 363 (2009) 135–142.
- [14] S. Xia, L. Zheng, L. Wang, P. Chen, Z. Hou, RSC Adv. 3 (37) (2013) 16569–16576.
- [15] J.I. Di Cosimo, V.K. Díez, C.R. Apesteguía, Appl. Catal. A: Gen. 13 (1996) 149–166.
- [16] S. Sato, R. Takahashi, T. Sodesawa, K. Yuma, Y. Obata, J. Catal. 196 (2000) 195–199.
- [17] P.A. Torresi, V.K. Díez, P.J. Luggren, J.I. Di Cosimo, Appl. Catal. A: Gen. 458 (2013) 119–129.
- [18] D.A. Monti, A. Baiker, J. Catal. 83 (1983) 323–335.
- [19] P. Malet, A. Caballero, J. Chem. Soc. Faraday Trans. I 84 (1988) 2369–2375.
- [20] C.J.G. Van Der Grint, A.F.H. Wielers, B.P.J. Jogh, J. Van Beijnum, M. De Boer, M. Versluijs-Helder, J.W. Geus, J. Catal. 131 (1991) 178–189.
- [21] P. Djinović, J. Batista, A. Pintar, Appl. Catal. A: Gen. 347 (2008) 23–33.
- [22] A. Gervasini, S. Bennici, Appl. Catal. A: Gen. 281 (2005) 199–205.
- [23] E.D. Guerreiro, O.F. Gorri, J.B. Rivarola, L.A. Arrúa, Appl. Catal. A: Gen. 165 (1997) 259–271.
- [24] G.C. Bond, S.N. Namijo, J. Catal. 118 (1989) 507–510.
- [25] E.L. Kunke, E.I. Gürbüz, J.A. Dumesic, J. Catal. 266 (2009) 236–249.
- [26] V.K. Díez, P.A. Torresi, P.J. Luggren, C.A. Ferretti, J.I. Di Cosimo, Catal. Today 213 (2013) 18–24.
- [27] C.A. Ferretti, A. Soldano, C.R. Apesteguía, J.I. Di Cosimo, Chem. Eng. J. 161 (2010) 346–354.
- [28] J.I. Di Cosimo, V.K. Díez, M. Xu, E. Iglesia, C.R. Apesteguía, J. Catal. 178 (1998) 499–510.
- [29] J.I. Di Cosimo, C.R. Apesteguía, J. Mol. Catal. 91 (1994) 369–386.
- [30] P. Djinovic, J. Levec, A. Pintar, Catal. Today 138 (2008) 222–227.

- [31] M. Xu, M.J.L. Gines, A. Hilmen, B.L. Stephens, E. Iglesia, *J. Catal.* 171 (1997) 130–147.
- [32] <http://abulafia.mt.ic.ac.uk>
- [33] H. Zhou, Z. Huang, C. Sun, F. Qin, D. Xiong, W. Shen, H. Xu, *Appl. Catal. B: Environ.* 125 (2012) 492–498.
- [34] P. Zimmer, A. Tschope, R. Birringer, *J. Catal.* 205 (2002) 339–345.
- [35] X. Tang, B. Zhang, Y. Li, Y. Xu, Q. Xin, W. Shen, *Appl. Catal. A: Gen.* 288 (2005) 116–125.
- [36] R.T. Sanderson, *Chemical Bonds and Bond Energy*, 2nd ed., Academic Press, New York, 1976.
- [37] J.I. Di Cosimo, C.R. Apesteguía, M.J.L. Ginés, E. Iglesia, *J. Catal.* 190 (2000) 261–275.
- [38] T.V. Choudhary, C.B. Phillips, *Appl. Catal. A: Gen.* 397 (2011) 1–12.
- [39] J.I. Di Cosimo, A. Acosta, C.R. Apesteguía, *J. Mol. Catal. A: Chem.* 234 (2005) 111–120.
- [40] F. Braun, J.I. Di Cosimo, *Catal. Today* 116 (2006) 206–215.